Finite Element Analysis of Piezoelectric Composite with Negative-stiffness Inclusions Considering Imperfect Bonding

Khin Lae Lae Oo[1] Yasothorn Sapsathiarn[1,*] and Yun-Che Wang[2]

[1] *Department of Civil and Environmental Engineering, Faculty of Engineering, Mahidol University, Nakhon Pathom, THAILAND*

[2] *Department of Civil Engineering, National Cheng Kung University, Tainan, TAIWAN*

**Corresponding author; E-mail address: yasothorn.sap@mahidol.ac.th*

Abstract

Piezoelectric materials, known for their electromechanical properties, are crucial in applications like structural health monitoring, sensors, actuators, and energy harvesting. This study presents a finite element-based micromechanical analysis to determine the effective properties of piezoelectric composites with varying fiber volume fractions. Boundary conditions for the representative volume element (RVE) are carefully examined to ensure periodicity and accuracy. The analysis is validated by comparing electromechanical coupling properties with previous studies. The study explores the potential of metamaterial properties in piezocomposites by incorporating negative-stiffness inclusions and considering the effect of imperfect bonding between the fiber and matrix. These factors can lead to unconventional mechanical behavior, such as enhanced flexibility or tunable stiffness, significantly improving performance for specific applications. By investigating these elements, the study offers valuable insights into the macroscopic properties of piezocomposites, essential for optimizing their design and performance across a wide range of engineering applications.

Keywords: Piezoelectric Composite, Finite Element Analysis, Micromechanics Analysis, Imperfect Bonding, Negative-Stiffness Inclusion

1. Introduction

Metamaterials are artificially engineered materials with unique properties not found in nature, designed to manipulate electromagnetic, acoustic, or seismic waves through their precise topology. Composed of metals and plastics in periodic patterns, they enable applications like electromagnetic cloaking, negative refraction, perfect absorption, and negative permeability [1]. Smart or piezoelectric materials, characterized by their electromechanical properties, operate via two mechanisms: the direct piezoelectric effect, converting mechanical energy into electrical energy for sensor applications, and the converse effect, converting electrical energy into mechanical deformation for actuators. Their brittleness and environmental limitations, leading to the development of piezoelectric composites. Research is increasingly focused on composite piezoelectric materials, which improve durability by embedding brittle piezoceramic fibers in flexible polymer matrices. These composite materials have applications in noise and vibration control, aerospace, energy harvesting, and structural health monitoring [2].

In composite material, the matrix (like polymer resin) serves to bond the reinforcing fiber (like ceramics or glass fiber) together. An imperfect interface that occurs due to the inconsistent adhesion between fiber and matrix leads to structural weakness. These imperfections can arise from various

issues such as fiber-matrix poor chemical incompatibility, inadequate surface treatment or manufacturing defects. A weak interface disrupts the load transfer between fiber and matrix while leading the stress concentration at the interface that might speed up material failure. In more severe cases, this can result in delamination and consequently cause complete structural failure. To analyze and tackle these interfacial imperfections, researchers use various methods. Some models treat the interface as a separate third phase with its own material properties [3], while others describe it through discontinuity conditions like spring or membrane type interface [4, 5], cohesive zone modeling [6], interface cracks [7] and thin layer interface model [8, 9]. Experimental techniques like single-fiber pull-out tests are also employed to assess interfacial strength.

Integrating negative-stiffness inclusions into composite materials presents an exciting opportunity to surpass the usual limits of mechanical properties. Unlike typical composites where properties remain bounded by those of the constituent materials, negative stiffness elements enable the creation of systems with extreme stiffness and damping characteristics, as shown by recent experimental and analytical research [10,11]. These inclusions can lead to properties that far surpass those of any single constituent even when the inclusion concentrations are low. These negative stiffness effects can come from various sources, such as solid-solid phase transitions, applied pre-stresses, or post-buckling behaviors [12]. In solid-solid phase transitions, the energy profile changes from positive to negative curvature at equilibrium, which gives to negative stiffness. Incorporating negative-stiffness elements into composite structures can produce remarkable mechanical effects, including increased stiffness, enhanced damping, and improved energy absorption. A conceptual model for a seismic metabarrier that includes a negative-stiffness dynamic vibration absorber aimed at reducing seismic impacts was proposed [13]. Recent parametric studies have revealed that innovative piezo-embedded negative stiffness metamaterials can greatly enhance both vibration attenuation and energy harvesting capabilities, as demonstrated by a spring-mass system model introduced to illustrate the concept of negative-stiffness metamaterials [14]. In [15], researchers found that the effective sensitivity of bimorph strip actuators was greatly improved by adding negative structural stiffness elements, which were created using post-buckled brass strips linked in series with the piezoelectric actuators. A negative stiffness element also triggers some unusual coupled-field responses like unexpected changes in thermal expansion, piezoelectricity, pyroelectricity, and electric permittivity [16].

The finite element-based micromechanical analysis is employed in this study to calculate effective properties of piezoelectric composites with varying fiber volume fractions and further to investigate the metamaterial properties by incorporating negative-stiffness inclusions into the composite. The insight understanding in this field is needed for creating novel high-performance composite designs.

2. Theoretical Background

2.1 Representative volume element (RVE)

In micromechanics theory, the representative volume element (RVE) is the smallest volume that sufficiently characterizes the overall properties of the material. The micromechanical approach analyzes the known properties of fiber and matrix in order to determine the effective properties of the piezoelectric fiber composites. This method is used to relate microstructural features to macroscopic properties. The selected representative unit cell for periodic fiber arrangement composites can be seen in Fig. 1.

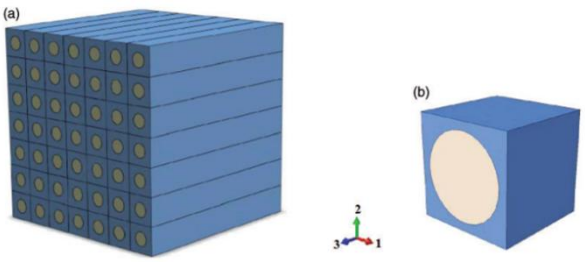

Fig. 1 (a) composite material and (b) representative unit cell [9]

The surfaces of RVE can be denoted as shown in Fig. 2 so that it can easily explain about loading and periodic boundary conditions on different surfaces. The axes numbers 1, 2 and 3 are equivalent to axes X, Y and Z respectively. The fiber is polarized along the Z-axis in all analyses.

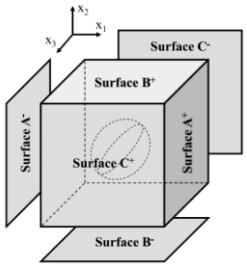

Fig. 2 Notation of the surfaces of the unit cell [17]

2.2 Constitutive equations of piezoelectric materials

The coupling properties of piezoelectric refer to the scenarios where mechanical deformation produces electrical energy (direct piezoelectric effect), whereas electric potential gradient transforms into mechanical energy (converse piezoelectric effect). The piezoelectric effect is defined as the inherent coupling between mechanical and electrical properties of a material, in terms of mechanical stress, strain, and electric field or charge. This interaction is represented by linear constitutive equations in the index notation as depicted in Eq. (1) (Stress-charge form) and Eq. (2) (Strain-charge form).

Stress-charge form:

$$\begin{aligned} T_{ij} &= C^{E}_{ijkl} S_{kl} - e_{kij} E_k \\ D_i &= e_{ikl} S_{kl} + \varepsilon^{S}_{ik} E_k \end{aligned} \tag{1}$$

Strain-charge form:

$$\begin{aligned} \varepsilon_{ij} &= S_{ijkl} \sigma_{kl} - d_{ijk} E_k \\ D_i &= d_{ijk} \sigma_{jk} + \dot{o}_{ij} E_j \end{aligned} \tag{2}$$

where (T_{ij} or $\boldsymbol{\sigma}_{kl}$) and (S_{ij} or $\boldsymbol{\varepsilon}_{ij}$) represent the 2nd-order stress and strain tensors, respectively, while E_k and D_i correspond to the electric field and electric displacement vectors. The 4th-order elasticity tensor and elastic compliance tensor are denoted as C_{ijkl} and S_{ijkl} correspondingly. The 3rd order piezoelectric coupling tensor in the stress-charge form is e_{kij}, while d_{ijk} is for the strain-charge form. Similarly, $\boldsymbol{\varepsilon}_{ik}$ and $\boldsymbol{\epsilon}_{ij}$ are the 2nd-order dielectric tensors for stress and strain forms.

Since the stress-charge and strain-charge formulations are largely similar except for certain symbol notations, the following equations and discussions will focus solely on the stress-charge form at a constant strain field.

The matrix format in Voigt's notation of Eq. (1) can be written as

$$\begin{bmatrix} T \\ D \end{bmatrix} = \begin{bmatrix} C^{E} & -e^{T} \\ e & \varepsilon^{S} \end{bmatrix} \begin{bmatrix} S \\ E \end{bmatrix} \tag{3}$$

where the superscript *T* represents the transpose of a matrix, while *E* denotes a constant electric field, and *S* signifies a constant strain field.

By applying Voigt's notation and simplifying the coefficients of the stiffness matrix, piezoelectric matrix, and dielectric matrix for a transversely isotropic piezoelectric solid, the constitutive equation for the piezoelectric composite can be represented in an expanded matrix form as shown in Eq. (4).

$$\begin{bmatrix} T_{11} \\ T_{22} \\ T_{33} \\ T_{23} \\ T_{13} \\ T_{12} \\ D_1 \\ D_2 \\ D_3 \end{bmatrix} = \begin{bmatrix} C^{E}_{11} & C^{E}_{12} & C^{E}_{13} & 0 & 0 & 0 & 0 & 0 & -e_{13} \\ C^{E}_{12} & C^{E}_{11} & C^{E}_{13} & 0 & 0 & 0 & 0 & 0 & -e_{13} \\ C^{E}_{13} & C^{E}_{13} & C^{E}_{33} & 0 & 0 & 0 & 0 & 0 & -e_{33} \\ 0 & 0 & 0 & C^{E}_{44} & 0 & 0 & 0 & -e_{15} & 0 \\ 0 & 0 & 0 & 0 & C^{E}_{44} & 0 & -e_{15} & 0 & 0 \\ 0 & 0 & 0 & 0 & 0 & C^{E}_{66} & 0 & 0 & 0 \\ 0 & 0 & 0 & 0 & e_{15} & 0 & \varepsilon^{S}_{11} & 0 & 0 \\ 0 & 0 & 0 & e_{15} & 0 & 0 & 0 & \varepsilon^{S}_{11} & 0 \\ e_{13} & e_{13} & e_{33} & 0 & 0 & 0 & 0 & 0 & \varepsilon^{S}_{33} \end{bmatrix} \begin{bmatrix} S_{11} \\ S_{22} \\ S_{33} \\ S_{23} \\ S_{13} \\ S_{12} \\ E_1 \\ E_2 \\ E_3 \end{bmatrix} \tag{4}$$

2.3 Periodic boundary conditions on unit cell

Composite materials can be modelled as a periodic array of representative volume elements (RVEs). In order to accurately describe the continuous physical structure of the arranged unit cells, continuity conditions must be satisfied at their boundaries. Firstly, the displacements should be continuous such that there should be no gap or overlap of the adjacent unit cells after the deformation. Lately, the traction distribution on the opposite parallel faces of a unit cell should be matched. Fig. 3 shows the displacement distribution on two opposite boundary surfaces.

The unit cell's configuration has been assumed that the fibers are continuous and uniformly distributed within the matrix to act periodically in all directions. Its average mechanical and electrical properties give a good representation of the whole composite material.

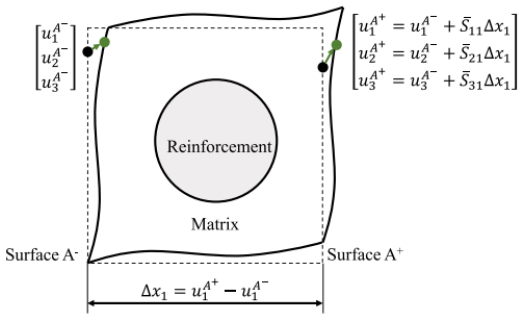

Fig. 3 Surface displacements [17]

To figure out the macroscopic average fields such as stress, strain, electric field, and electric displacement the volume averaging method as shown in Eq. (5) is used. These calculations are crucial for understanding how the composite behaves mechanically within the representative volume element (RVE), shedding light on its performance when subjected to mechanical loads.

$$\begin{aligned}\bar{S}_{ij} &= \tfrac{1}{V}\int_V S_{ij}dV \\ \bar{E}_{ij} &= \tfrac{1}{V}\int_V E_{ij}dV \\ \bar{T}_{ij} &= \tfrac{1}{V}\int_V T_{ij}dV \\ \bar{D}_{ij} &= \tfrac{1}{V}\int_V D_{ij}dV\end{aligned} \quad (5)$$

The overall effective properties of composites are governed by the material properties of the constituents, the fiber volume fraction of the inclusions, negative-stiffness inclusion and the nature of the interface bonding.

2.4 Negative-stiffness inclusion

In elastic materials, the characteristic of the material deforms in the same direction as the force applied is called positive stiffness. In contrast, negative stiffness refers to the scenario where the applied force and the resulting movement are in opposite directions. Negative stiffness can occur when the deformed object stores energy or receives energy from outside, often due to structural instability mechanisms such as buckling or phase transformations. This unstable situation can be stabilized by embedding negative-stiffness inclusion into positive-stiffness matrix. That kind of composite can lead to extremely high or low effective coupled-field properties [18, 19]. Additionally, the bonding condition between fiber and matrix may also be another factor that can affect the properties of the piezoelectric composite with negative-stiffness inclusion.

2.5 Imperfect fiber-matrix interface

The impact of imperfect interfaces may be more significant in the composite with negative-stiffness inclusions. Here, stress concentrations at the interface can amplify local instabilities, which in turn affects the overall mechanical behavior of the material. In order to get accurate predictions about the effective properties of piezoelectric composite with negative-stiffness inclusion, it is crucial to choose the right interface model and implement it properly in simulation software. Among the various models used to present imperfect fiber-matrix bonding, the present study proposes the thin interface model as the preferred methodology for characterizing interfacial behavior.

For an isotropic interface, normal traction T_n and tangential traction T_t rely on the respective normal displacement jump $[u_n]$ and tangential displacement jump $[u_t]$ that occurs across the interface. The interface conditions can be expressed as

$$T_n = K_n[u_n] \quad \text{and} \quad T_t = K_t[u_t] \quad (6)$$

where K_n and K_t are normal and tangential direction contact behaviors described in terms of spring constants per unit area (interface parameters).

The interface is perfect when K_n and K_t increase indefinitely and the displacement discontinuities vanish. In contrast, a fully debonded interface occurs when K_n and K_t approach to zero and the interfacial tractions diminish. The coefficients for the interface with thickness t are calculated by using Hashin's interface model [9] as follows:

$$
\begin{aligned}
&K_n = \frac{t}{\lambda + 2G}, K_t = \frac{t}{G} \\
&C_{11} = C_{22} = C_{33} = \lambda + 2\mu \\
&C_{12} = C_{13} = C_{23} = \lambda \\
&C_{44} = C_{55} = C_{66} = \mu = \frac{C_{11} + C_{12}}{2} \\
&\lambda = t(K_n - 2K_t) \\
&\mu = G
\end{aligned} \tag{7}
$$

3. Numerical Model Implementation

3.1 Boundary condition implementation

The proper boundary conditions to the representative volume element (RVE) are needed in order to figure out the effective coefficients. Each effective coefficient can be calculated by multiplying the corresponding row of the material matrix with the strain or electric field vector after setting all but one component of the strain or electric field vector in Eq. (4) to zero. This whole process is made easier by enforcing the appropriate boundary conditions and constraint equations on the different surfaces of the RVE [20].

For example, to evaluate the effective coefficients e_{13}, e_{33}, e_{33}, it needs to make sure that all surfaces are constrained to avoid any normal displacement. A zero electric potential is applied to the surface C^+ whereas a nonzero electric potential to surface C^-. The electric potential on all other surfaces set to zero. With displacement constraints on all surfaces and an electric potential difference applied along the x_3 direction, the fiber expands, creating both mechanical stresses and electric fields in the same direction. Under this condition, the last row of the matrix in Eq. (4) simplifies to the following expression:

$$
e_{13}^{eff} = -\frac{T_{11}}{E_3}, \quad e_{33}^{eff} = -\frac{T_{33}}{E_3} \quad \text{and} \quad \varepsilon_{13}^{eff} = \frac{D_3}{E_3} \tag{8}
$$

The simulation was carried out using COMSOL Multiphysics and the resulting electromechanical responses were compared with those from the earlier studies. Fig. 4 shows the model geometry that was used to assess the effective properties of the piezoelectric composite based on the assumption of a perfectly bonded fiber-matrix interface. Meanwhile, Fig. 5 illustrates the model utilized to investigate the G_{xz} modulus anomaly in piezoelectric materials with negative-stiffness inclusion.

The effective G_{xz} can be evaluated by assigning constant shear stresses in the opposite direction on the X^+ and Z^+ surfaces while enforcing antisymmetry conditions on the X^- and Z^- surfaces. Additionally, the electric potential condition on all six surfaces of the cube is set to zero [16]. The expression for Gxz modulus is as follow:

$$
G_{xz} = C_{44} = \frac{T_{13}}{S_{13}} \tag{9}
$$

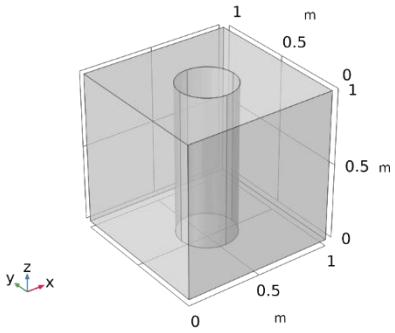

Fig. 4 Piezocomposite with 0.111 fiber volume fraction for perfect interface bonding

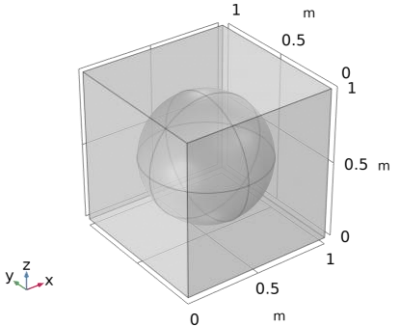

Fig. 5 Model for piezoelectric with negative-stiffness inclusion

3.2 Material properties

The cylindrical fiber (PZT-5) is embedded in the polymer matrix with the consideration of a perfectly bonded fiber-matrix interface. The effective properties of the piezoelectric composite for six different fiber volume fractions, which range from 0.111 to

0.666 in steps of 0.111. The material properties used in this analysis can be found in Table 1.

In the case of analysis relating to the negative-stiffness inclusion, the parameters and material properties used are summarized in Table 2 and Table 3. The inclusion is spherical with the radii of 0.2 m and 0.4 m and exhibits negative-stiffness behavior, which is modelled by assigning a negative bulk modulus ratio. This approach allows for the investigation of the impact of negative-stiffness inclusions on the effective properties of the composite material.

Table 1 Material properties of fiber (PZT-5) and matrix (polymer) [20]

	PZT-5	Polymer
C_{11} (GPa)	121	3.86
C_{12} (GPa)	75.4	2.57
C_{13} (GPa)	75.2	2.57
C_{33} (GPa)	111	3.86
C_{44} (GPa)	21.1	0.64
C_{66} (GPa)	22.8	0.64
e_{15} (C/m^2)	12.3	-
e_{13} (C/m^2)	-5.4	-
e_{33} (C/m^2)	15.8	-
$\boldsymbol{\varepsilon}_{11}$ (nCV/m)	8.11	0.07965
$\boldsymbol{\varepsilon}_{33}$ (nCV/m)	7.35	0.07965

Table 2 Parameters for negative-stiffness inclusion analysis [19]

	Matrix	Inclusion
Geometry	Cube (1x1x1 m3)	Sphere Radius = 0.2, 0.4 m
Inclusion volume ratio (%)	-	26.8
Material properties	PZT-5H or PZT-7A	Isotropic elastic solid
Young's modulus, *E*	Anisotropic elastic compliance of piezoelectric	$E_i = \lambda_E E_{ref}$ $\left(E_{ref} = 110GPa\right)$ $V_i = 0.33$
Bulk modulus, *K*	Anisotropic elastic compliance of piezoelectric	$K_i = \lambda_K K_{ref}$ $\left(K_{ref} = 100GPa\right)$ $G_i = 25GPa$

Table 3 Material properties of PZT-5H and PZT-7A

	PZT-5H	PZT-7A
C_{11} (GPa)	127.205	157.701
C_{12} (GPa)	80.2122	87.6735
C_{13} (GPa)	84.6702	81.2032
C_{33} (GPa)	117.436	125.688
C_{44} (GPa)	22.9885	29.4118
C_{66} (GPa)	23.4742	34.965
e_{15} (C/m^2)	17.0345	10.5882
e_{13} (C/m^2)	-6.62281	-2.2984
e_{33} (C/m^2)	23.2403	9.48595
$\boldsymbol{\varepsilon}_{11}$ (nCV/m)	0.151	4.42
$\boldsymbol{\varepsilon}_{33}$ (nCV/m)	0.127	2.04
Density (kg/m^3)	7500	7700

*** Built in material properties in COMSOL Multiphysics*

4. Results and discussion

The effective piezoelectric coefficient e_{13} of the piezoelectric composite, consisting of PZT-5 fibers embedded in a polymer matrix, is analyzed under the assumption of perfect bonding at the fiber-matrix interface. According to the boundary conditions set by Berger et al., [20], the effective properties of piezoelectric composite obtained by the present simulation are consistent with the results from Berger et al., which validate the results of finite element method with the analytical method, for different loading cases except when it comes to an applied electric field E_3. Under the applied E_3, the simulation results initially differed from those reported by Berger et al. [20], despite adopting the same boundary conditions - zero normal displacement on all surfaces, zero electric potential on surface C^- and non-zero electric potential on surface C^+. This deviation is attributed to electric field variations along the x_3 direction, inducing fiber expansion. To account for this effect, additional displacement constraints were imposed on the fiber surfaces, as summarized in Table 4, by setting the x_2 displacement and electric potential to zero on the fiber surface. Following these modifications, the results exhibited close agreement with those of Berger et al. [20]. The comparison results between the present study and the reference results from Berger et al., are represented in Fig. 6 to Fig. 8. The detailed comparison for effective properties of e_{13} with different fiber volume fraction can be summarized in Table 5.

Table 4 Boundary condition for electric field E_3 case

A^+ & A^-	B^+ & B^-	C^+ & C^-
$u_1 = 0$ $u_2 = free$ $u_3 = free$	$u_1 = free$ $u_2 = 0$ $u_3 = free$	$u_1 = free$ $u_2 = free$ $u_3 = 0$
$\Phi = 0$	$\Phi = 0$	$\Phi = 1(C^+ surface)$ $\Phi = 0(C^- surface)$
Constraints on fiber surfaces: $u_1 = free,\ u_2 = 0,\ u_3 = free,\ \Phi = 0$		

** u *denotes a prescribed displacement*

** Φ *denotes a prescribed electric potential*

Fig. 6 clearly shows the downward trend in the effective e_{13} coefficient as the fiber volume fraction goes up. However, the gap between the two datasets becomes more noticeable at higher fiber volume fractions. The deviations at higher fiber volume fractions are attributed to stronger local fields and increased fiber-to-fiber interactions associated with high fiber densities. As the volume fraction increases, these effects become more pronounced and are not fully captured by the simplified assumptions in homogenization, leading to discrepancies with the reference results. The present data consistently reports lower values compared to the reference data. On the other hand, the comparison graphs in Fig. 7 and Fig. 8 demonstrate consistent results between the present study and the reference data that is concerning the evolution of the effective piezoelectric and dielectric constants as a function of varying fiber volume fractions. This consistency highlights how the reliability of the current numerical approach is when it comes to predicting these material properties. This finding emphasizes the need for mechanical constraints on fiber-matrix interface.

Table 5 Comparison for effective coefficient e_{13}

V_f	Present Study (1)	Reference (2)	Difference (%)
0.111	-0.0281	-0.0243	15.64
0.222	-0.0661	-0.0569	16.17
0.333	-0.1195	-0.0990	20.71
0.444	-0.1992	-0.1601	24.42
0.555	-0.3300	-0.2533	30.28
0.666	-0.5888	-0.4356	35.17

*** Difference (%) = [[(1)-(2)]/(2)]*100*

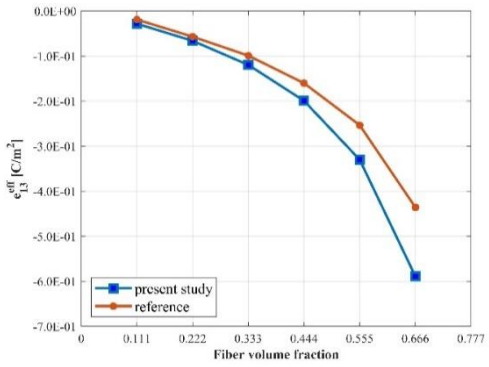

Fig. 6 Effective piezoelectric constant (e_{13}) Vs fiber volume fraction

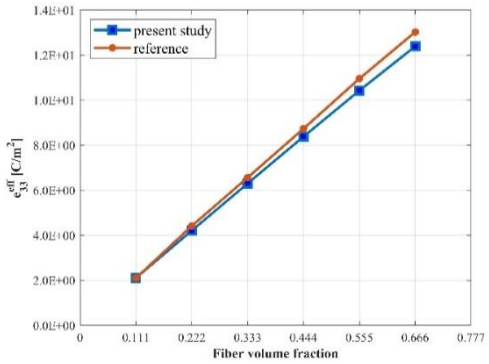

Fig. 7 Effective piezoelectric constant (e_{33}) Vs fiber volume fraction

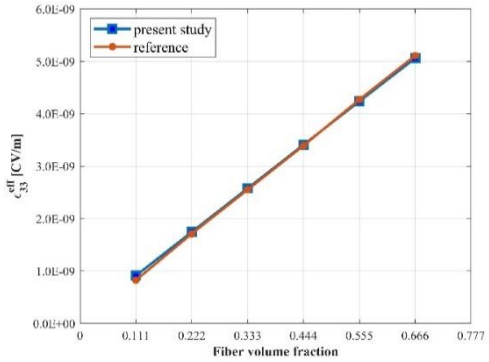

Fig. 8 Effective dielectric constant (ε_{33}) Vs fiber volume fraction

To evaluate the effective properties of piezoelectric materials that include negative-stiffness inclusions, the comparison between the present study (PZT-7A) and the reference data (PZT-5H) [16] is conducted, which have different dielectric properties that can influence their mechanical response. This analysis examines spherical inclusions with radii of 0.2 m and 0.4 m as shown in Fig. 9 and Fig. 10. From the figures,

the greater inclusion size shows the fluctuations in the less negative region of modulus ratio. A higher inclusion volume fraction results the appearance of more peaks. This occurrence is consistent with the description in the reference data [16]. On the other hand, PZT-7A, which permittivity value is higher than that of PZT-5H, gives the fluctuation in more negative region in different inclusion size. This finding indicates that inclusion size and dielectric properties play a crucial role in the mechanical stability of these materials.

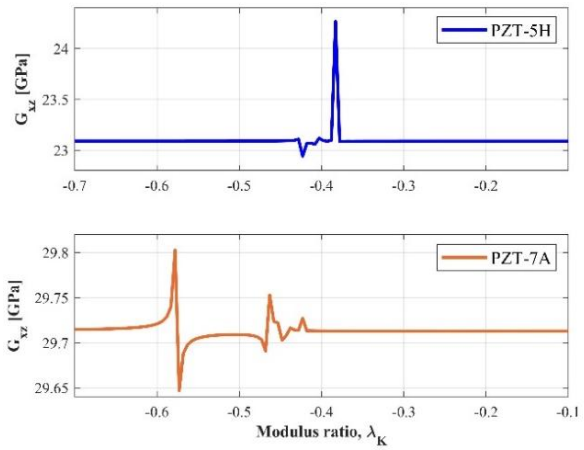

Fig. 9 Effective shear modulus versus the inclusion modulus ratio for spherical radius 0.2 m

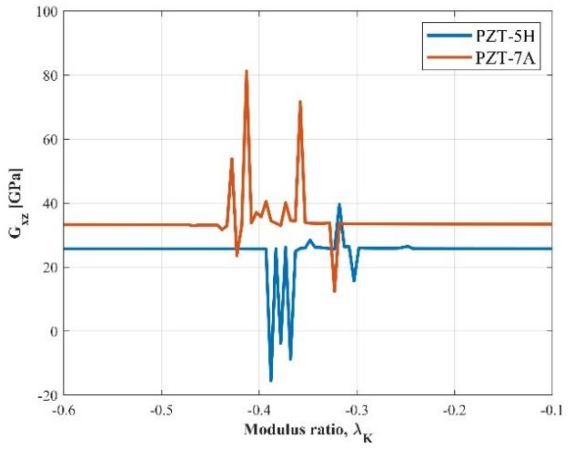

Fig. 10 Effective shear modulus versus the inclusion modulus ration for spherical radius 0.4 m.

5. Conclusions

The present study highlights the influence of several parameters like fiber-matrix interface, inclusion size, and selection of piezoelectric material type on the effective properties of piezoelectric composites. Even negative-stiffness inclusion consideration leads to the possibilities for metamaterial design, those unusual peaks create some challenges with the system instabilities.

Future research should focus on the stability analysis to define the system stability boundary and choose the right fiber-matrix interface models for evaluating the effect of bonding imperfections. Integrating the approach of imperfect bonding effects with negative-stiffness inclusions will help develop more efficient piezoelectric composites through advanced modelling.

6. Acknowledgements

This work was supported by Mahidol University, Thailand Science Research and Innovation (TSRI) and National Science, Research and Innovation Fund (NSRF), Grant No. FF-136/2568 and Taiwan National Science and Technology Council (NSTC 112-2221-E-006-049-MY3) with the New South Policy.

References

[1] Huang, W., Li, C., Fang, B., Xu, J., Liu, F., Xu, L., Tang, Y., Hong, Z., & Jing, X. (2024). Research progress of terahertz wave dynamic control of digital coded metasurfaces. Optics and Lasers in Engineering, 174, 107977.

[2] Mahapatra, S. Das, Mohapatra, P. C., Aria, A. I., Christie, G., Mishra, Y. K., Hofmann, S., & Thakur, V. K. (2021). Piezoelectric Materials for Energy Harvesting and Sensing Applications: Roadmap for Future Smart Materials. Advanced Science, 8(17).

[3] Kordkheili, H., & Toozandehjani, H. (2014). Effective mechanical properties of unidirectional composites in the presence of imperfect interface. Archive of Applied Mechanics, 84(6), 807–819.

[4] Shi, Y., Wan, Y., & Zhong, Z. (2017a). Anti-plane time-harmonic Green's functions for a coated circular inhomogeneity in a piezoelectric medium with spring- or membrane-type imperfect interfaces. Mathematics and Mechanics of Solids, 22(9), 1813–1846.

[5] Shi, Y., Wan, Y., & Zhong, Z. (2017b). Dynamic effective property of fibrous piezoelectric composites with spring- or membrane-type imperfect interfaces. Mechanics Research Communications, 84, 116–124.

[6] Tarafder, P., Dan, S., & Ghosh, S. (2023). Cohesive zone phase field model for electromechanical fracture in multiphase piezoelectric composites. Journal of Composite Materials, 57(4), 531–544.

[7] Sapsathiarn, Y., Senjuntichai, T., & Rajapakse, R. K. N. D. (2012). Cylindrical interface cracks in 1-3 piezocomposites. Composites Part B: Engineering, 43(5), 2257–2264.

[8] Brito-Santana, H., de Medeiros, R., Rodriguez-Ramos, R., & Tita, V. (2016). Different interface models for calculating the effective properties in piezoelectric composite materials with imperfect fiber–matrix adhesion. Composite Structures, 151, 70–80.

[9] Tita, V., De Medeiros, R., Marques, F. D., & Moreno, M. E. (2015). Effective properties evaluation for smart composite materials with imperfect fiber-matrix adhesion. Journal of Composite Materials, 49(29), 3683–3701.

[10] Wang, Y. C., Ko, C. C., Chang, K. W., & Ko, T. W. (2021). Negative-stiffness composite systems and their coupled-field properties. Continuum Mechanics and Thermodynamics, 33(4), 1857–1872.

[11] Wang, Y. C., & Lakes, R. S. (2004). Extreme stiffness systems due to negative stiffness elements. American Journal of Physics, 72(1), 40–50.

[12] Wang, Y. C., Wu, C. Y., & Kuo, Q. Y. (2011). Negative stiffness of a buckled carbon nanotube in composite systems via molecular dynamics simulation. Physica Status Solidi (B) Basic Research, 248(1), 88–95.

[13] Lin, S., Zhang, Y., Liang, Y., Liu, Y., Liu, C., & Yang, Z. (2021). Bandgap characteristics and wave attenuation of metamaterials based on negative-stiffness dynamic vibration absorbers. Journal of Sound and Vibration, 502.

[14] Dwivedi, A., Banerjee, A., & Bhattacharya, B. (2020). Simultaneous energy harvesting and vibration attenuation in piezo-embedded negative stiffness metamaterial. Journal of Intelligent Material Systems and Structures, 31(8), 1076–1090.

[15] Kalathur, H., & Lakes, R. (2016). Enhancement in piezoelectric sensitivity via negative structural stiffness. Journal of Intelligent Material Systems and Structures, 27(18), 2568–2573.

[16] Wang, Y. C., & Lakes, R. S. (2001). Extreme thermal expansion, piezoelectricity, and other coupled field properties in composites with a negative stiffness phase. Journal of Applied Physics, 90(12), 6458–6465.

[17] Ferreira, P. M., Machado, M. A., Vidal, C., & Carvalho, M. S. (2024). Modelling electro-mechanical behaviour in piezoelectric composites: Current status and perspectives on homogenisation. In Advances in Engineering Software (Vol. 193). Elsevier Ltd.

[18] Lakes, R. S. (2001). Extreme damping in composite materials with a negative stiffness phase. Physical Review Letters, 86(13), 2897–2900.

[19] Wang, Y. C., Ko, C. C., & Chang, K. W. (2015). Anomalous effective viscoelastic, thermoelastic, dielectric, and piezoelectric properties of negative-stiffness composites and their stability. Physica Status Solidi (B) Basic Research, 252(7), 1640–1655.

[20] Berger, H., Kari, S., Gabbert, U., Rodriguez-Ramos, R., Guinovart, R., Otero, J. A., & Bravo-Castillero, J. (2005). An analytical and numerical approach for calculating effective material coefficients of piezoelectric fiber composites. International Journal of Solids and Structures, 42(21–22), 5692–5714.